IEEE Access
Multidisciplinary | Rapid Review | Open Access Journal

Received 4 August 2023, accepted 21 August 2023, date of publication 24 August 2023, date of current version 30 August 2023.

Digital Object Identifier 10.1109/ACCESS.2023.3308491

RESEARCH ARTICLE

Parameter Sensitivity Analysis and Optimization of Electromagnetic Force Waves of Fractional Slot Surface-Mounted PM Motor With External Rotor

JIAKUAN XIA, MEIJUN QI, TING DONG, AND MENGLIN SONG
School of Electrical Engineering, Shenyang University of Technology, Shenyang 110870, China

Corresponding author: Meijun Qi (qimeijun77@163.com)

This work was supported in part by the National Natural Science Foundation of China under Grant 52177054.

ABSTRACT For PM motor with external rotor, the electromagnetic force wave acting on the surface of the permanent magnet by the air gap magnetic field is the main cause of its electromagnetic vibration. In this paper, an optimization method based on parameter sensitivity for electromagnetic force wave of fractional slot surface-mounted PM motor with external rotor is proposed. Firstly, taking a fractional slot surface-mounted PM motor with external rotor as the research object, Latin Hypercube Design (LHD) is carried out with six structural parameters as design variables, including pole arc coefficient, notch width, air gap length, permanent magnet thickness, tooth width and slot depth, and the parameter sensitivity of different design variables to the average torque and the main radial electromagnetic force wave amplitude is analyzed. Secondly, based on the experimental results of Latin Hypercube Design, a mathematical approximation model is established by using radial basis function neural network method. Then, with the aim of improving the average torque and reducing the amplitude of the main radial electromagnetic force wave, neighborhood cultivation genetic algorithm is applied to optimize the structure of the motor. Finally, the optimized motor scheme is simulated by finite element simulation to verify the feasibility and accuracy of the proposed method.

INDEX TERMS PM motor with external rotor, radial electromagnetic force wave, parameter sensitivity, Latin hypercube design, radial basis function neural network, neighborhood cultivation genetic algorithm.

I. INTRODUCTION

Fractional slot surface-mounted PM motor has the advantages of short winding end, high torque density, high efficiency, high power density, good servo performance and fault tolerance [1], [2], [3]. It has been widely used in NC rotary table, precision robot, electric vehicle, submarine propulsion, wind power generation and other fields [4], [5], [6], [7], [8]. Compared with integer slot PM motors, fractional slot PM motors have lower spatial order of electromagnetic force and electromagnetic vibration and noise problems are more prominent [9], [10], [11]. Electromagnetic force wave is the main source of electromagnetic vibration of motors, the quantitative calculation and analysis of the law of electromagnetic force wave is the basis for the study of electromagnetic vibration of motors [12], [13] Unlike the PM motor with inner rotor, the electromagnetic vibration of the PM motor with external rotor is caused by the electromagnetic force acting on the surface of the permanent magnet by the air gap magnetic field [14], [15]. In this paper, the prototype is a turntable motor, which has strict requirements on electromagnetic vibration and torque density. Therefore, it is necessary to analyze and optimize the electromagnetic force of the fractional slot surface-mounted PM motor with external rotor for NC rotary table.

At present, there are mainly analytic method and numerical method to study the electromagnetic force. The analytic method obtains the air gap flux density by solving the partial differential equation, and then obtains the radial electromagnetic force wave analytic expression by using Maxwell

The associate editor coordinating the review of this manuscript and approving it for publication was Frederico Guimarães.

stress tensor method [16]. However, it is difficult to take into account the complex tooth and slot structure of the stator, magnetic circuit saturation and other factors by the analytic method, and the accuracy of the calculation results is low. Finite element method can accurately get each component of the electromagnetic force density, but the optimization process requires several iterations of the finite element model, which will consume a lot of time and cost.

At present, there are many studies on electromechanical force of PM motor at home and abroad. In [10], for PM motor with similar number of poles and slots, the vibration and noise of the motor is further reduced by the stator tooth chamfering. In [15], for external rotor PM motor, the electromagnetic force is reduced by optimizing the notch width. In [17], a method of slotting the auxiliary slot on the stator tooth is proposed to change the number of slots and poles in fractional slot PM motor to further weaken the electromagnetic force wave. In [18], for the interior PM motor and the surface-mounted PM motor, the electromagnetic force is reduced by the skewed slots. In [19] and [20], the electromagnetic force is effectively reduced and the electromagnetic noise is suppressed by optimizing the pole arc coefficient. However, the above literatures only analyze the effect of changes in a single parameter on the electromagnetic force.

In [21], for inner rotor PM motor, the air gap length is optimized by simultaneously changing the outer diameter of rotor and the inner diameter of stator, so as to weaken the electromagnetic force. For the interior PM brushless DC motor, in [22], the electromagnetic force in further weakened by optimizing the diameter of the rotor notch, the angle of the stator chamfering and the direction of magnetization. In [23], for surface-mounted PM brushed DC motor, the optimization of electromagnetic force is carried out by the number of poles/slots and pole arc coefficient. The above literatures consider several parameters when optimizing the electromagnetic force, but most of them only consider the influence of each parameter on the electromagnetic force, ignore the simultaneous changes of each parameter, it can't obtain the optimal solution of parameter combination, and the parameterized optimization using only finite element model takes a lot of work. Therefore, this paper establishes and optimizes a mathematical model between the structure parameters and the average torque and the amplitude of the main radial electromagnetic force wave, taking into account several motor structure parameters, which greatly reduces the calculation time and obtains the optimal solution of the set motor structure parameter combination. In addition, this paper analyzes and optimizes the main radial electromagnetic force wave of a specific spatial order and frequency of the largest electromagnetic vibration except o space order 0Hz. Compared with the above literatures, this paper has a more specific research objective and more significant effect.

This paper proposes an optimal design method for electromagnetic force wave of fractional slot PM motor based on parameter sensitivity. Parameter sensitivity analysis of different parameters is carried out by designing 3Latin Hypercube test. On this basis, RBF neural network algorithm is used to establish a mathematical approximate model, and NCGA is used to optimize the motor structure parameters. Finally, the feasibility and accuracy of the proposed method are verified by finite element method, which provides a basis for designing a fractional slot surface-mounted PM motor with external rotor for NC rotary table and reducing vibration and noise under complex operating conditions.

II. THE MODEL OF FRACTIONAL SLOT SURFACE-MOUNTED PM MOTOR WITH EXTERNAL ROTOR

This paper takes a fractional slot surface-mounted PM motor with external rotor for NC rotary table as an example to analyze. The main parameters and structure of the motor are shown in Table 1 and Fig. 1.

TABLE 1. Main parameters of motor.

Specifications	Values
Number of poles and slots	48/54
Rated power, kW	1.15
Rated speed, r/min	60
Outer diameter of rotor, mm	290
Inner diameter of rotor, mm	274
Permanent magnet thickness, mm	3
Air gap length, mm	1
Inner diameter of stator, mm	197
Core length, mm	110
Pole arc coefficient	0.97

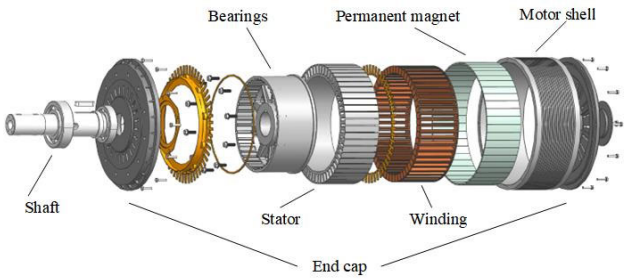

FIGURE 1. Structure of the motor.

Existing literatures are sufficient to demonstrate the high accuracy of the finite element simulation [24], [25]. To verify the accuracy of the finite element simulation calculation, the back EMF of the motor at the rated speed of 60 r/min is measured by test. The test platform is shown in Fig. 2. The line voltage measured by the test is compared with that calculated by the finite element simulation as shown in Fig. 3. It can be seen that the test result and the FEM result are basically the same.

III. CALCULATION AND ANALYSIS OF ELECTROMAGNETIC FORCE WAVE

For surface-mounted PM motor, the effective air gap length is large, and the magnetic circuit is generally unsaturated. When the PM motor is running, the permanent magnet magnetic

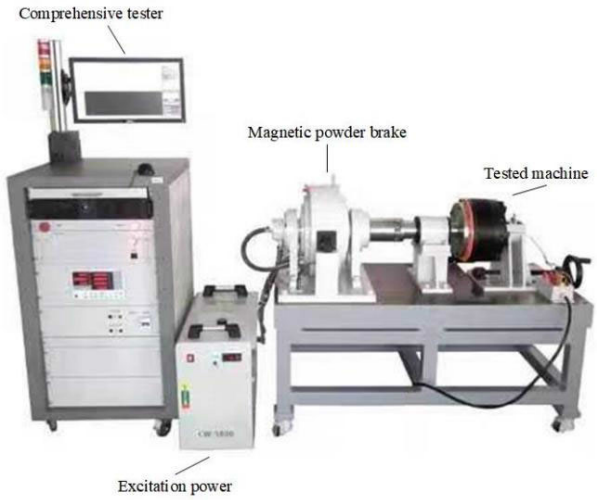

FIGURE 2. The test platform.

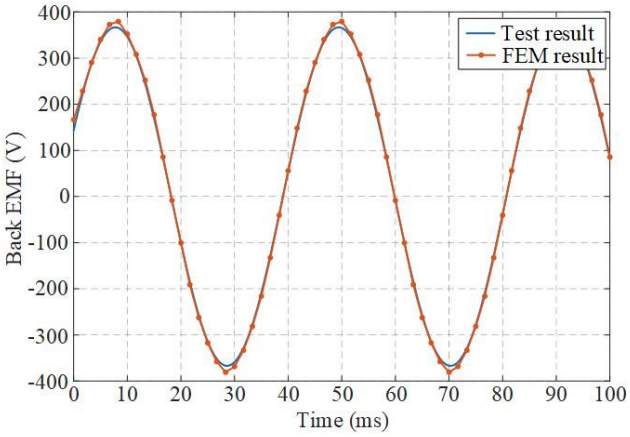

FIGURE 3. Line voltage comparison result.

field and the armature reaction field interact to produce the air gap magnetic field. Ignoring magnetic circuit saturation, the synthetic radial flux density B_r is

$$B_r = \left(F_{r\_mag} + F_{r\_arm}\right)\lambda_\delta \tag{1}$$

According to Maxwell tensor method, the radial electromagnetic force P_r can be expressed as

$$P_r = \frac{1}{2\mu_0}\left(B_r^2 - B_t^2\right) \tag{2}$$

where, μ_0 is the vacuum permeability. Ignoring the effect of tangential flux density B_t, the radial electromagnetic force can be expressed as

$$P_r = \frac{B_r^2}{2\mu_0} \tag{3}$$

For PM motor with external rotor, the rotor is a noise radiator, and the electromagnetic vibration is caused by the electromagnetic force acting on the surface of the permanent magnet by the air gap magnetic field. Therefore, in this paper, the radial electromagnetic force acting on the internal surface of the permanent magnet is mainly studied. The coordinate system is fixed on the rotor coordinate system, assumes that the external rotor is fixed and the stator rotates in the opposite direction with an angular velocity. The expressions of radial permanent magnet magnetomotive force F_{r_mag}, radial armature magnetomotive force F_{r_arm} and specific permeability λ_δ are respectively given

$$F_{r\_mag} = \sum_{\mu} F_{m\mu}\cos\left(\mu p\theta\right) \tag{4}$$

$$\begin{aligned} F_{r\_arm} &= \sum_{\upsilon} F_{a\upsilon}\sin\left[\upsilon N_t\left(\theta + 2\pi f_r t\right) - 2\pi s_\upsilon f_1 t\right] \\ &= \sum_{\upsilon} F_{a\upsilon}\sin\left[\upsilon N_t\theta - 2\pi\left(s_\upsilon p_0 - \upsilon\right)N_t f_r t\right] \end{aligned} \tag{5}$$

$$\lambda_\delta = \lambda_0 + \sum_{n}\lambda_{\delta n}\cos\left(nQ_s\theta + 2\pi nQ_s f_r t\right) \tag{6}$$

where, $F_{m\mu}$ is the amplitude of the radial permanent magnet magnetomotive force in μ^{th} harmonic permanent magnet field, $F_{a\upsilon}$ is the amplitude of radial armature magnetomotive force in υ^{th} armature reaction magnetic field, p is the number of pole pairs, p_0 is the number of the number of unit motor's pole pairs, Q_s is the number of slots, θ is the spatial angle, t is time, N_t is the space period of the motor (also known as the number of unit motor), f_1 is the fundamental frequency of current, $f_1 = p \times f_r$, f_r is the rotating frequency, s_υ is the rotation direction of the υ^{th} harmonic of the armature reaction magnetic field, -1 is positive rotation, 1 is reverse rotation, λ_0 is the average air-gap permeance, $\lambda_{\delta n}$ is the amplitude of the n^{th} harmonic permeance.

In order to further deduce the characteristics of the electromagnetic force acting on the surface of permanent magnet, the radial armature magnetomotive force is further simplified

$$F_{r\_arm} = \sum_{\upsilon} F_{a\upsilon}\sin\left[\upsilon N_t\theta - 2\pi \times 3kN_{pQ_s}f_r t\right] \tag{7}$$

where, N_{pQs} is the greatest common divisor GCD $(2p, Q_s)$ of the number of poles and slots of the motor. By substituting formula (4), (6) and (7) into formula (1) and (3), the radial electromagnetic force acting on the surface of the permanent magnet can be obtained as

$$\begin{aligned} P_r &= \frac{1}{2\mu_0}\{\sum_{\mu} F_{m\mu}\cos\left(\mu p\theta\right) \\ &\quad + \sum_{\upsilon} F_{a\upsilon}\sin[\upsilon N_t\theta - 2\pi 3kN_{pQ_s}f_r t]\}^2 \\ &\quad \times [\lambda_0 + \sum_{n}\lambda_{\delta n}\cos\left(nQ_s\theta + 2\pi nQ_s f_r t\right)]^2 \\ &= \frac{1}{4\mu_0}\{\sum_{\mu_1}\sum_{\mu_2} F_{m\mu_1}F_{m\mu_2}[\cos\left(\mu_1 + \mu_2\right)p\theta \\ &\quad + \cos\left(\mu_1 - \mu_2\right)p\theta] \\ &\quad + 2\sum_{\mu}\sum_{\upsilon} F_{m\mu}F_{a\upsilon}\{\sin[\left(\mu p + \upsilon N_t\right)\theta - 2\pi 3kN_{pQ_s}f_r t] \\ &\quad - \sin[\left(\mu p - \upsilon N_t\right)\theta + 2\pi 3kN_{pQ_s}f_r t]\} \end{aligned}$$

TABLE 2. Source, amplitude, spatial order, and frequency of radial electromagnetic force wave on the surface of permanent magnet.

Source	Amplitude	Spatial order	Frequency
Permanent magnet magnetic field	$\frac{1}{4\mu_0}\lambda_0^{\,2}F_{\mathrm{m}\mu_1}F_{\mathrm{m}\mu_2}$	$(\mu_1 \pm \mu_2)\,p$	0
Armature reaction magnetic field	$\frac{1}{4\mu_0}\lambda_0^{\,2}F_{\mathrm{a}\nu_1}F_{\mathrm{a}\nu_2}$	$(\nu_1 \pm \nu_2)\,N_{\mathrm{t}}$	$3(k_1 \pm k_2)\,N_{pQ_{\mathrm{s}}}f_r$
Interaction between permanent magnet magnetic field and armature reaction magnetic field	$\frac{1}{2\mu_0}\lambda_0^{\,2}F_{\mathrm{m}\mu}F_{\mathrm{a}\nu}$	$np \pm \nu N_{\mathrm{t}}$	$3kN_{pQ_{\mathrm{s}}}f_r$
Interaction between permanent magnet magnetic field and slotted stator	$\frac{1}{4\mu_0}\lambda_0\lambda_{\delta n}F_{\mathrm{m}\mu_1}F_{\mathrm{m}\mu_2}$	$(\mu_1 \pm \mu_2)\,p \pm nQ_{\mathrm{s}}$	$nQ_{\mathrm{s}}f_{\mathrm{r}}$
	$\frac{1}{16\mu_0}\lambda_{\delta n_1}\lambda_{\delta n_2}F_{\mathrm{m}\mu_1}F_{\mathrm{m}\mu_2}$	$(\mu_1 \pm \mu_2)\,p \pm (n_1 \pm n_2)\,Q_{\mathrm{s}}$	$(n_1 \pm n_2)\,Q_{\mathrm{s}}f_{\mathrm{r}}$
Interaction between armature reaction magnetic field and slotted stator	$\frac{1}{4\mu_0}\lambda_0\lambda_{\delta n}F_{\mathrm{a}\nu_1}F_{\mathrm{a}\nu_2}$	$(\nu_1 \pm \nu_2)\,N_{\mathrm{t}} \pm nQ_{\mathrm{s}}$	$3(k_1 \pm k_2)\,N_{pQ_{\mathrm{s}}}f_{\mathrm{r}} \pm nQ_{\mathrm{s}}f_{\mathrm{r}}$
	$\frac{1}{16\mu_0}\lambda_{\delta n_1}\lambda_{\delta n_2}F_{\mathrm{a}\nu_1}F_{\mathrm{a}\nu_2}$	$(\nu_1 \pm \nu_2)\,N_{\mathrm{t}} \pm (n_1 \pm n_2)\,Q_{\mathrm{s}}$	$3(k_1 \pm k_2)\,N_{pQ_{\mathrm{s}}}f_{\mathrm{r}} \pm (n_1 \pm n_2)\,Q_{\mathrm{s}}f_{\mathrm{r}}$
Interaction between permanent magnet magnetic field, armature reaction magnetic field and slotted stator	$\frac{1}{2\mu_0}\lambda_0\lambda_{\delta n}F_{\mathrm{m}\mu}F_{\mathrm{a}\nu}$	$(np \pm \nu N_{\mathrm{t}}) \pm nQ_{\mathrm{s}}$	$3kN_{pQ_{\mathrm{s}}}f_{\mathrm{r}} \pm nQ_{\mathrm{s}}f_{\mathrm{r}}$
	$\frac{1}{8\mu_0}\lambda_{\delta n_1}\lambda_{\delta n_2}F_{\mathrm{m}\mu}F_{\mathrm{a}\nu}$	$(\mu p \pm \nu N_{\mathrm{t}}) \pm (n_1 \pm n_2)\,Q_{\mathrm{s}}$	$3kN_{pQ_{\mathrm{s}}}f_{\mathrm{r}} \pm (n_1 \pm n_2)\,Q_{\mathrm{s}}f_{\mathrm{r}}$

$$
\begin{aligned}
&+\sum_{\nu_1}\sum_{\nu_2}F_{\mathrm{a}\nu_1}F_{\mathrm{a}\nu_2}\{\cos[(\nu_1-\nu_2)\,N_t\theta\\
&-2\pi 3\,(k_1-k_2)\,N_{pQ_{\mathrm{s}}}f_{\mathrm{r}}t]-\cos[(\nu_1+\nu_2)\,N_t\theta\\
&-2\pi 3\,(k_1+k_2)\,N_{pQ_{\mathrm{s}}}f_{\mathrm{r}}t]\}\}\\
&\times\{\lambda_0^2+2\lambda_0\sum_{n}\lambda_{\delta n}\cos\,(nQ_{\mathrm{s}}\theta+2\pi nQ_{\mathrm{s}}f_{\mathrm{r}}t)\\
&+\frac{1}{2}\sum_{n_1}\sum_{n_2}\lambda_{\delta n_1}\lambda_{\delta n_2}\{\cos[\,(n_1+n_2)\,Q_{\mathrm{s}}\theta\\
&+2\pi\,(n_1+n_2)\,Q_{\mathrm{s}}f_{\mathrm{r}}t]+\cos[(n_1-n_2)\,Q_{\mathrm{s}}\theta\\
&+2\pi\,(n_1-n_2)\,Q_{\mathrm{s}}f_{\mathrm{r}}t]\}\}
\end{aligned}
\tag{8}
$$

As can be seen from Table 2, when armature reaction magnetic field is not taken into account, i.e. under no-load, the frequency of the electromagnetic force generated by the interaction between the permanent magnet magnetic field and the slotted stator is $k \times Q_{\mathrm{s}} \times f_{\mathrm{r}}$, which is the integer multiple of the number of slots. Under load, the frequency of the electromagnetic force is $k \times 3N_{pQ\mathrm{s}} \times f_{\mathrm{r}}$, which is the integer multiple of 3 times the greatest common divisor of the number of poles and slots. In this paper, the pole-slot match of the motor is 48/54, and the winding form is fractional slot concentrated double-layer winding. The motor is spatially equivalent to six 8/9 motors, i.e., the number of spatial period N_{t} is six, the number of pole pairs p_0 and slots Z_0 of the unit motor are 4 and 9 respectively, satisfying $Z_0 = 2\,p_0 \pm 1$, N_{t} equals $N_{pQ\mathrm{s}}$, and the harmonic order of armature reaction magnetic field $\upsilon = 3k \pm 1$.

The finite element model of the motor is established in Maxwell 2D to obtain the radial air gap flux density when the motor is under no-load and load, and the result of 2-D Fourier decomposition of the radial air gap flux density when the motor is under no-load and load is obtained after processing, as shown in Fig. 4.

From Fig. 4, it can be seen that the amplitude and fluctuation of air gap flux density under load are larger than that under no-load, and the logarithm of harmonic poles after 2-D Fourier decomposition under no-load and load are both p, and the amplitude of each order has little difference. This paper considers the effect of armature reaction magnetic field, so the analysis is mainly focused on the load. The radial electromagnetic force wave under load and its 3-D Fourier space-time decomposition result are shown in Fig. 5.

According to Table 2, under load condition, armature reaction magnetic field is taken into account. The load condition has additional $k \times 18$ Hz electromagnetic force waves compared to the no-load condition, but their values are smaller, and the electromagnetic force waves at $k \times 54$ Hz (slot frequency) have a greater effect. Therefore, the electromagnetic force waves at $k \times 2p$ space order, $k \times 54$ Hz is the main source of vibration. From Fig. 5, it can be seen that the radial electromagnetic force wave is mainly concentrated in the 0 space order 0 Hz, $2p$ space order 54 Hz, $4p$ space order 108 Hz and $6p$ space order 162 Hz, which is consistent with the theoretical analysis result. The 0 space order 0 Hz electromagnetic force wave is generated by the interaction of the stator's own harmonic magnetic field and the rotor's own harmonic magnetic field. Considering that the amplitude of the fundamental magnetic field in a normally designed motor is much greater than that of the harmonic magnetic field, the 0 space order 0 Hz electromagnetic force wave is mainly generated by the fundamental magnetic field. Due to

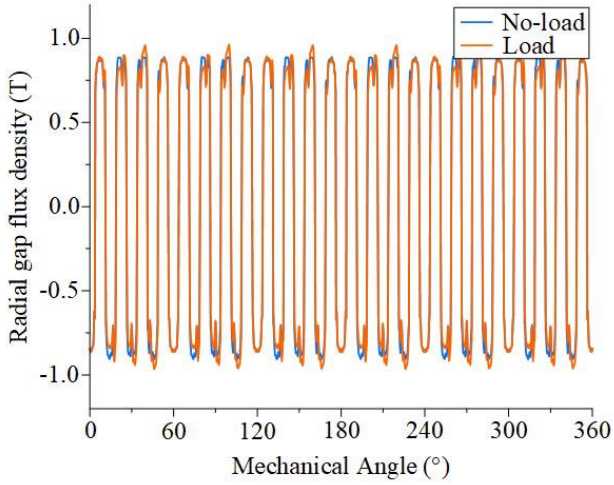

(a) Radial air gap flux density

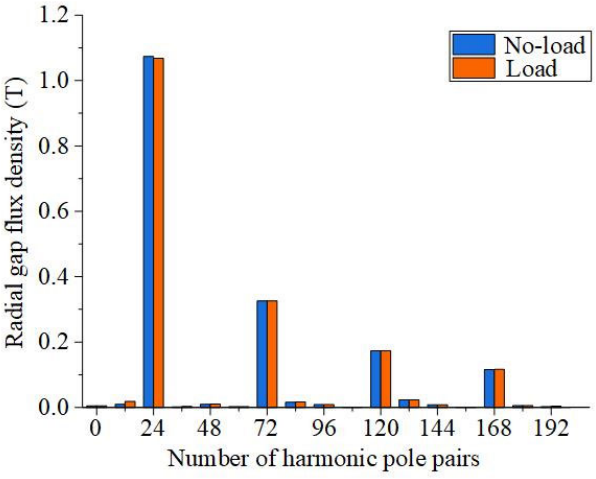

(b) Radial air gap flux density's 2-D Fourier decomposition

FIGURE 4. Radial air gap flux density and its 2-D Fourier decomposition.

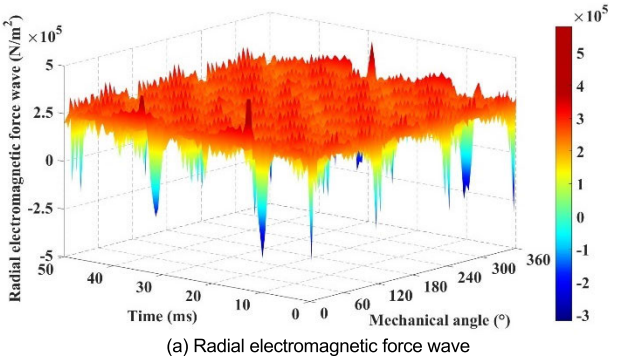

(a) Radial electromagnetic force wave

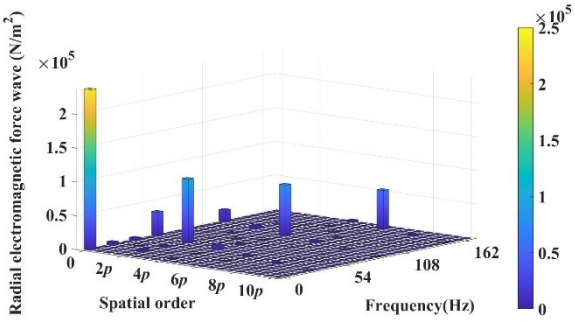

(b) Radial electromagnetic force wave's 3-D Fourier space-time decomposition

FIGURE 5. The radial electromagnetic force wave and its 3-D Fourier space-time decomposition.

the 0 space order 0 Hz electromagnetic force wave being 0, it will not cause electromagnetic vibration and noise.Therefore, the radial electromagnetic force wave of $2p$ space order 54 Hz has the greatest effect on the vibration noise of the motor. Electromagnetic vibration can be effectively weakened by reducing the amplitude of the major electromagnetic force wave. The armature reaction magnetic field is considered in this study. Therefore, the $2p$ space order 54 Hz radial electromagnetic force wave under load will be analyzed below.

IV. PARAMETER SENSITIVITY ANALYSIS OF THE MAIN RADIAL ELECTROMAGNETIC FORCE WAVE

A. ANALYSIS OF DIFFERENT STRUCTURAL PARAMETERS AND THEIR INFLUENCE

The factors that affect the electromagnetic force wave include the electromagnetic parameters and structural parameters, both of which affect electromagnetic force wave by changing the air gap magnetic field. In this paper, six structural parameters including pole arc coefficient, notch width, air gap length, permanent magnet thickness, tooth width and slot depth are selected for analysis. Fig. 6. shows the motor topology diagram with six parameter positions labelled. The size of these six structural parameters directly affects the distribution of the air gap magnetic field, which in turn affects the radial electromagnetic force wave and the average torque, as shown in Fig. 7.

Fig. 7 shows the influence of six structural parameters on the amplitude of main electromagnetic force wave and average torque. It can be seen that when the pole arc coefficient is between 0.55 and 1, the amplitude of the radial electromagnetic force wave decreases and the average torque increases with increasing the pole arc coefficient. When the air gap length is between 0.4mm and 1.4mm, the amplitude of the radial electromagnetic force wave decreases and the average torque increases with decreasing the air gap length. The notch width has little effect on the average torque, but the amplitude of the radial electromagnetic force wave increases approximately linearly in range. The influence of permanent magnet thickness, tooth width and slot depth on the amplitude of main electromagnetic force wave and average torque is similar with the increase of the value. The inflection points in subplot (d) and subplot (f) are both caused by the flux density supersaturation. Because the rated speed of the prototype in this paper is low, considering the cost, the design of the yoke flux density is relatively high. In subplot (e), when tooth width is 6mm, the flux density has reached saturation. It can be seen that the variation of the pole arc coefficient

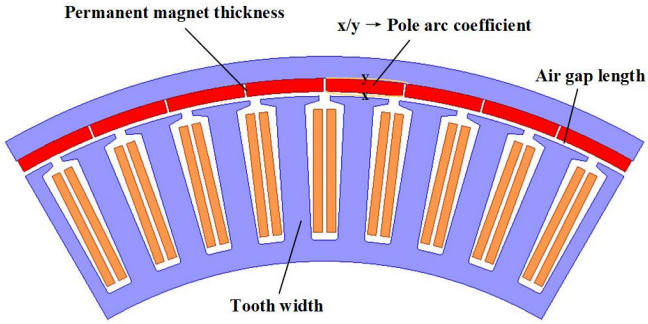

(a) Topological diagram of the motor on a two-dimensional plane

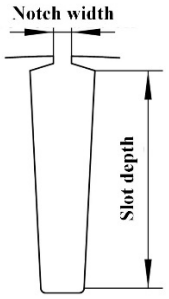

(b) Enlarged view of stator slot

FIGURE 6. Topological diagram of the motor.

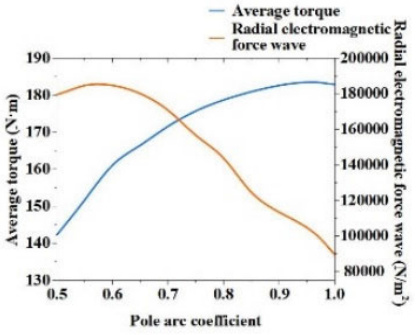

(a) The impact trend of pole arc coefficient

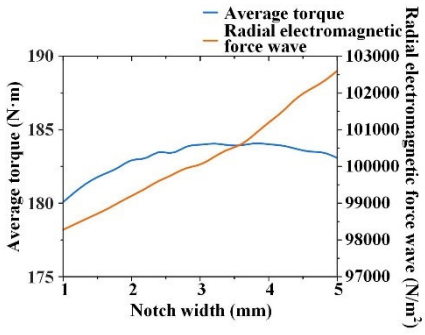

(b) The impact trend of notch width

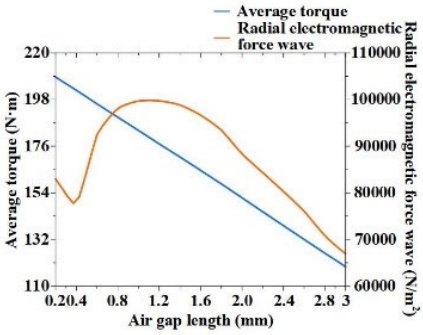

(c) The impact trend of air gap length

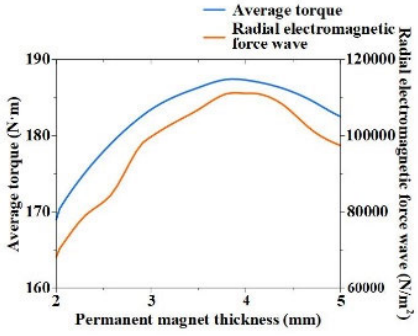

(d) The impact trend of permanent magnet thickness

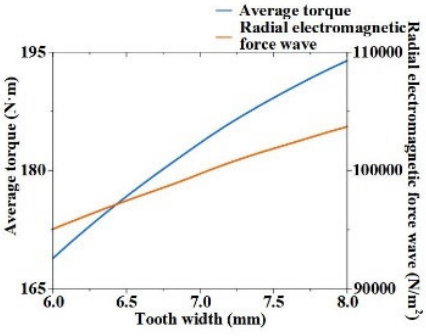

(e) The impact trend of tooth width

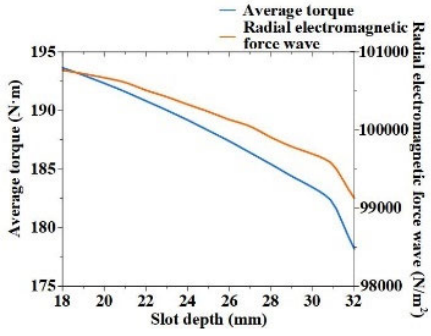

(f) The impact trend of slot depth

FIGURE 7. The influence of different structural parameters on the amplitude of main electromagnetic force wave and average torque.

and the air gap length within the range proposed in this paper is beneficial to the reduction of the amplitude of main electromagnetic force wave and the increase of the average torque. On the basis of considering mechanical and cost issues, six parameter ranges are selected, and finally the range of pole arc coefficient is 0.8 ∼1, the range of notch width is 2∼4mm, the range of air gap length is 0.6∼1.4mm, the range of permanent magnet thickness is 2∼4mm, the range of tooth width is 6∼8mm and the range of slot depth is 28∼32mm.

B. TEST DESIGN

Design of Experiments (DOE) is one of the most important statistical methods in product development, process optimization and so on. It is based on the theory of mathematical statistics to scientifically arrange test schemes so as to correctly analyze test results and quickly obtain optimization schemes. This paper uses Latin hypercube design (LHD) method to select the number of points randomly and ensure that each level of a factor is studied only once. This method can effectively fill the space and fit the nonlinear response. The LHD factor and its constraint range are shown in Table 3.

Based on the parameterized finite element model established above and the designed LHD factor and its constraint range, 50 sample points are randomly selected for independent finite element load simulation. The average torque and radial electromagnetic force wave corresponding to each sample point are obtained. Then the radial electromagnetic force wave is decomposed by Fourier transformation to obtain the $2p$ space order 54 Hz radial electromagnetic force wave. The average torque T and the $2p$ space order 54 Hz

TABLE 3. Parameters and constraint range of LHD.

Parameters	Symbol	Initial values	Constraint range
Pole arc coefficient	a	0.97	0.8~1
Notch width, (mm)	b	2.5	2~4
Air gap length, (mm)	c	1	0.6~1.4
Permanent magnet thickness, (mm)	d	3	2~4
Tooth width, (mm)	e	7	6~8
Slot depth, (mm)	f	30	28~32

TABLE 4. LHD matrix and response results.

Serial number	a	b	c	d	e	f	T	F_r
1	0.80	3.0	1.4	2.1	6.8	29.6	148.53	95644
2	0.80	2.0	0.9	2.7	6.1	28.3	166.23	131470
3	0.81	2.2	1.3	2.5	6.9	28.7	161.70	113150
4	0.81	4.0	1.4	3.2	6.9	29.7	167.31	128210
5	0.82	2.3	1.0	2.3	6.7	30.2	167.20	111830
6	0.82	2.5	0.6	3.1	7.2	30.9	194.60	152020
7	0.82	3.3	0.9	2.2	7.1	31.8	171.45	114840
8	0.83	2.2	1.3	3.6	6.3	31.8	165.41	133970
9	0.83	3.2	0.7	2.9	6.8	28.5	186.80	137580
10	0.84	2.9	0.7	3.1	7.2	31.6	191.12	138340
.				.				.
.				.				.
.				.				.
40	0.96	2.2	1.2	3.8	7.3	28.8	184.78	108710
41	0.96	2.7	0.9	2.4	7.4	30.6	184.30	85579
42	0.97	2.0	0.8	3.9	6.6	32.0	182.38	105190
43	0.97	2.8	0.8	2.4	6.0	28.1	170.38	79440
44	0.98	3.8	1.2	2.3	7.6	28.2	171.43	79154
45	0.98	2.4	1.0	2.9	6.1	28.7	170.17	86695
46	0.98	2.7	0.6	3.0	7.5	31.0	202.77	89272
47	0.99	3.1	1.4	3.1	6.4	29.3	166.26	90328
48	0.99	3.8	1.4	3.0	7.6	31.5	173.29	95665
49	1.00	2.1	0.7	2.2	6.7	29.0	180.57	70694
50	1.00	2.7	1.1	2.1	7.7	28.9	172.70	76433

radial electromagnetic force wave F_r are taken as output responses. The final LHD matrix and response results are shown in Table 4.

C. PARAMETER SENSITIVITY ANALYSIS

Parameter sensitivity analysis refers to the sensitivity of the system's output to changes in input, which can be approximated as the contribution of factors to the response. The six factors $a \sim f$ are normalized to $[-1,1]$ and fitted with the least square method to get sensitivity S_i, which is then converted into percentage Nx_i

$$N_{x_i} = 100 \times \frac{S_{x_i}}{\sum_i |S_{x_i}|} \tag{9}$$

Table 5 shows the parameters sensitivity analysis results of six factors $a \sim f$ to average torque T and radial electromagnetic force wave F_r respectively, and the corresponding bar charts are shown in Fig. 8 and Fig. 9.

Sensitivity level I is classified as having absolute sensitivity greater than 10%, and sensitivity level II as having less than 10%. From the parameters sensitivity analysis results, it can be seen that the air gap length and the permanent magnet thickness have a greater influence on the average torque and radial electromagnetic force wave, which are all sensitivity level I. The pole arc coefficient has a greater effect on the radial electromagnetic force wave, but a smaller effect on the average torque. The sensitivity levels are II and I respectively. The tooth width has a greater effect on the average torque, but has less effect on the radial electromagnetic force wave. The sensitivity levels are I and II respectively. Notch width and slot depth have little effect on average torque

TABLE 5. Parameter sensitivity analysis results.

Parameters	N-T (%)	N-F_r (%)	Sensitivity level
a	5.47	-42.12	II/I
b	1.54	2.38	II/II
c	-35.38	-12.14	I/I
d	25.14	35.22	I/I
e	28.98	6.55	I/II
f	-3.48	-1.59	II/II

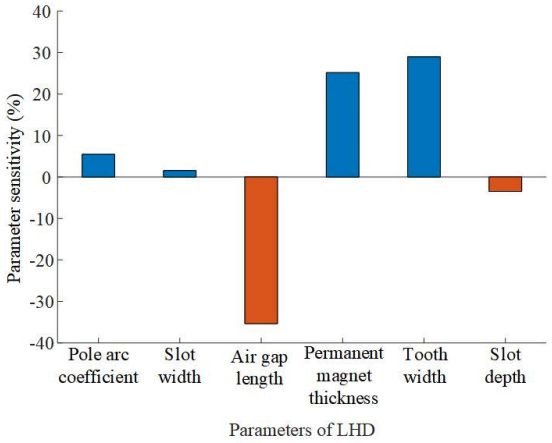

FIGURE 8. The parameters sensitivity analysis results of T.

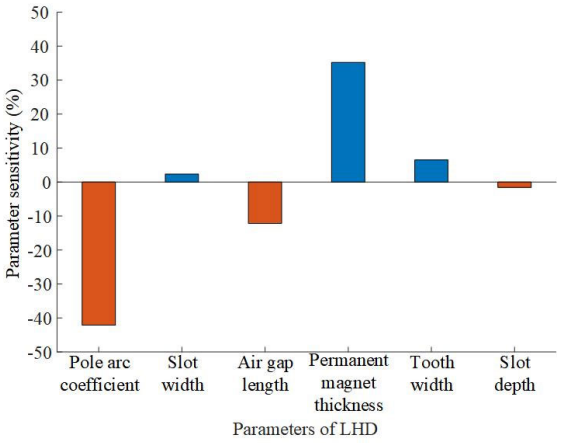

FIGURE 9. The parameters sensitivity analysis results of F_r.

and radial electromagnetic force wave, both of which are sensitivity levels II.

V. APPROXIMATE MODEL ANALYSIS BASED ON ARTIFICIAL NEURAL NETWORK METHOD

Artificial neural network method is based on the traditional statistical theory and has great advantages in dealing with problems with fuzzy information and many factors. Radial Basis Function (RBF) neural network method is a forward network constructed on the basis of the function approximation theory. It can approximate any continuous function with any precision and has a strong function approximation ability.

Based on the Latin hypercube test results (50 samples), the RBF neural network method is adopted to establish the approximate model between the pole arc coefficient, notch width, air gap length, permanent magnet thickness, tooth width, slot depth and the average torque and the amplitude of radial electromagnetic force wave. The number of RBF neural network layers is 3, which are input layer, hidden layer, and output layer. The corresponding number of nodes are 6, 10 and 2. Where the number of hidden layer nodes is selected based on previous experience. In order to verify the accuracy of the approximate model and obtain a reliable mathematical proxy model, 20 sample points are randomly selected, cross-validation method is used for error analysis, and the relative error and R^2 are used as the standard to measure the accuracy of the approximate model.

The relative error can be expressed as

$$E_i = \frac{|\hat{y}_i - y_i|}{y_i} \times 100\% \tag{10}$$

The expression for R^2 is

$$R^2 = 1 - \frac{\sum_i (y_i - \hat{y}_i)^2}{\sum_i (y_i - \bar{y}_i)^2} \tag{11}$$

where, y_i is the actual value, $\hat{y}_i$ is the predictive value, $\bar{y}_i$ is the average value. The smaller relative error, the greater R^2 is 0.9 and the closer it is to 1, the higher accuracy and reliability of the approximation model. The relative error and the calculated results of R^2 are shown in Table 6. The R^2 graphs of average torque T and radial electromagnetic force wave F_r are shown in Fig. 10 and Fig. 11.

In the R^2 graphs, the blue line is the average of the actual values of the 20 sampling points, the 45° slanted black line represents $R^2 = 1$, when the predictive value is equal to the actual value, the red dots are the predictive and actual values of the 20 sampling points. From Table 6, it can be seen that the relative error of radial electromagnetic force wave F_r is more than 5% for only 3 sampling points and less than 5% for average torque T for 20 sampling points. Therefore, the approximate model established by using RBF neural network method in this paper is reliable and can be used for subsequent optimization design.

TABLE 6. Relative error and R^2 calculation results.

Sample points	T-relative error (%)	T-R^2	F_r-relative error (%)	F_r- R^2
1	0.1038		9.1749	
2	0.2329		1.6271	
3	0.0444		2.0170	
4	0.2239		4.9690	
5	0.1137		2.9604	
6	0.3327		1.3654	
7	0.3266		0.8161	
8	0.5479		0.2116	
9	0.1790		1.6023	
10	0.2235		1.1895	
11	0.4098	0.97092	0.5091	0.96822
12	2.2193		10.5921	
13	1.1894		3.6178	
14	0.1775		2.0825	
15	0.3616		1.3682	
16	0.8350		0.0735	
17	3.3420		1.1816	
18	0.3635		4.2156	
19	0.1080		5.0138	
20	0.5273		2.1335	

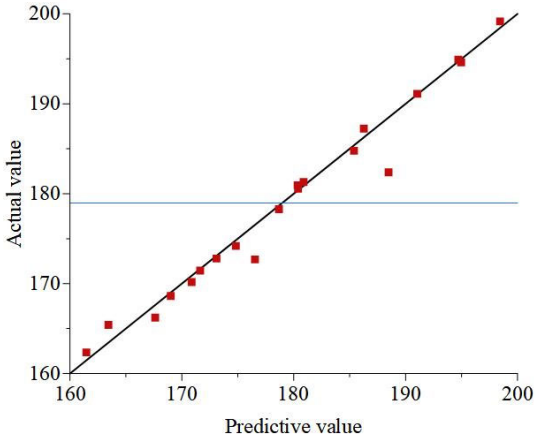

FIGURE 10. The R^2 graphs of average torque T.

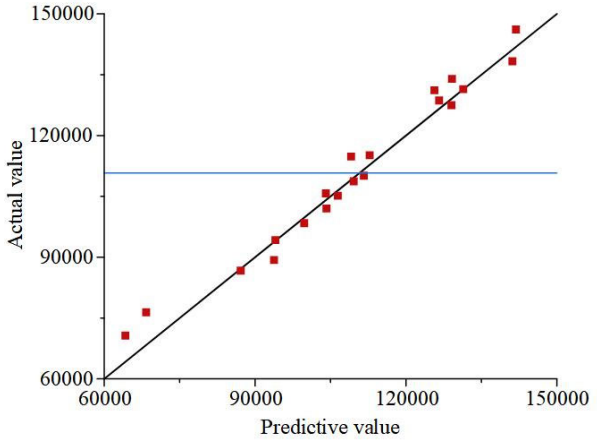

FIGURE 11. The R^2 graphs of radial electromagnetic force wave F_r.

VI. OPTIMIZATION DESIGN BASED ON NCGA

Multi-Objective Optimization is the problem of simultaneously optimizing multiple subgoals. Neighborhood

Cultivation Genetic Algorithm (NCGA) is developed from the earliest GA (Genetic Algorithm), which considers each target equally important and implements the mechanism of ''adjacent propagation'' through sorting and grouping for crossover. The mechanism of ''adjacent propagation'' increases the probability of crossbreeding solutions close to the Pareto frontier and accelerates the process of calculation convergence, but cannot solve single objective problems and has weak adaptability. This algorithm originates from the concept of subpopulations in distributed genetic algorithms, which limit the crossover to a certain range in the design space. According to the characteristics of the algorithm, the crossover between populations (neighborhoods) with similar characteristics is more effective. In most cases, each sub objective often conflicts with each other, and the improvement of a certain sub objective may lead to the reduction of other sub objectives. Thus, NCGA cannot optimize multiple sub objectives simultaneously, ultimately can only coordinate the trade-offs and compromises between objectives, so that each sub objective can be optimized as much as possible. Compared to traditional algorithms, NCGA supports optimization solutions for nonlinear and inequality constrained problems, it has fast operation speed, high reliability of calculation results, and fast convergence. The NCGA calculation process is shown in Fig. 12.

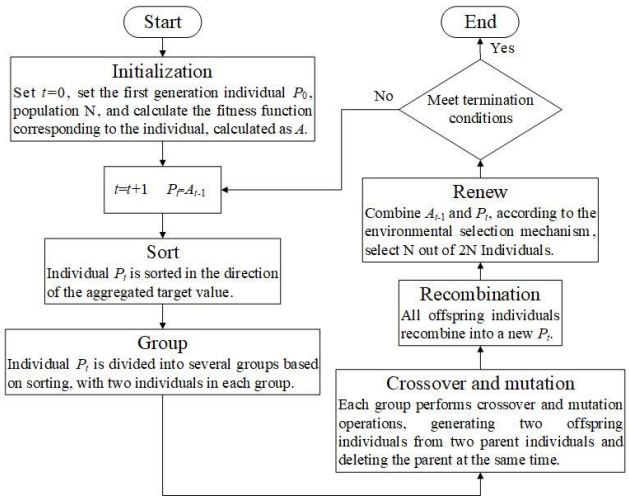

FIGURE 12. NCGA calculation process.

In this paper, the approximate model established by RBF neural network method and NCGA is used to optimize the design of the motor. During the optimization process, the change of structural parameters will lead to the change of slot area. Since only six structural parameters are changed in this paper, it is necessary to ensure that the slot fill factor s differs little from the original scheme and is less than 75%, so the constraint is set to $70\% < s < 75\%$. Set the population size to be 100, the crossover probability to be 0.7, the mutation probability to be 0.000 5, the number of iterations to be 2000, and the optimization target to be the minimum radial electromagnetic force wave and the maximum average torque.

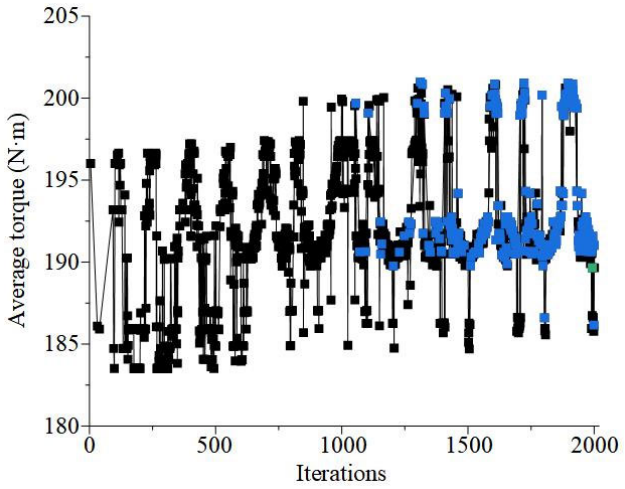

FIGURE 13. The iterative process of average torque.

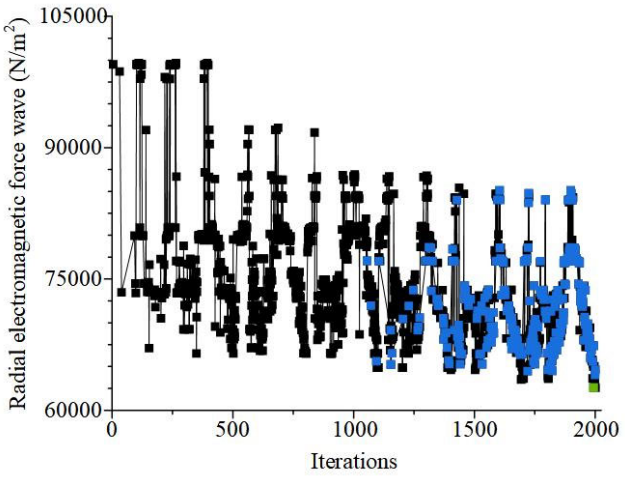

FIGURE 14. The iterative process of radial electromagnetic force wave.

TABLE 7. Comparison between NCGA and FEM.

Parameters	NCGA	FEA	Error(%)
a	0.999709		
b	3.133402		
c	0.605331		
d	2.07843		
e	7.16993		
f	30.77675		
Slot fill factor (%)	70.89705	70.532	0.518
Average torque (N·m)	189.6568	189.7532	0.051
Radial electromagnetic force wave (N/m^2)	62601.79	65731.74	4.762

Fig. 13 and Fig. 14 show the iterative process of average torque and radial electromagnetic force wave optimization respectively, and the optimal scheme is obtained by iterating to 1993 times.

Fig. 15 is the Pareto frontier in the optimization process. In Fig. 13, Fig. 14 and Fig. 15, the black points are the

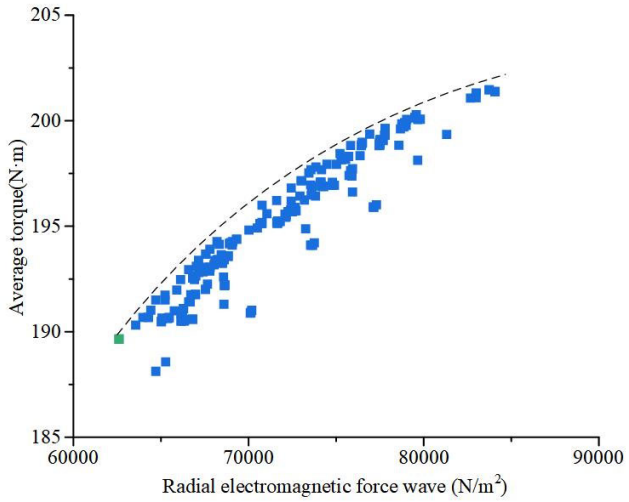

FIGURE 15. The Pareto frontier.

TABLE 8. Comparison of results before and after optimization.

Parameters	Initial values	After optimization	Comparison(%)
Slot fill factor (%)	70.2249	70.8187	0.846
Cogging torque (N·m)	6.89695	3.13567	-54.535
Average torque (N·m)	183.4368	190.3952	3.793
Torque ripple (%)	7.2357	6.6929	-7.502
Efficiency (%)	90.563	91.375	0.897
Overload multiple	1.6978	1.7087	0.642
Radial electromagnetic force wave (N/m2)	99693	71297	-28.483

feasible solutions, the blue points are the Pareto solutions, and the green points are the optimal solutions. It can be seen that the amplitude of the main radial electromagnetic force wave and the average torque cannot reach the optimal value at the same time. Therefore, the minimum value of the main radial electromagnetic force wave can only be obtained if the average torque is not lower than the initial value of 183.4368N.m.

The motor optimization scheme obtained by NCGA is compared with that by FEM simulation as shown in Table 7.

From Table 7, it can be seen that the errors of slot fill factor, average torque and amplitude of main radial electromagnetic force wave obtained by NCGA optimization are 0.518%, 0.051% and 4.762% respectively, when the motor parameters are input into the finite element simulation. Thus, the results obtained by NCGA have high accuracy and can be used as the final optimization scheme. However, there are many decimal places, considering the actual processing and other issues, so rounding is carried out on the basis of the optimization scheme obtained by NCGA. All parameters except the pole arc coefficient which retains two decimal places are retained one decimal place. The final optimization scheme is obtained by further finite element simulation. The comparison of the optimization results is shown in Table 8.

As can be seen from Table 8, the optimization method used in this paper has a high reliability, with an improved average torque of 3.793 %, efficiency of 0.897 %, overload multiple of 0.642 % and a reduced cogging torque of 54.535 %, torque ripple of 7.502 %, amplitude of major radial electromagnetic force wave of 28.483 %.

VII. CONCLUSION

In this paper, firstly, a parametric finite element simulation model of a fractional slot surface-mounted PM motor with external rotor is established. Secondly, the LHD test is designed and the parameters sensitivity of six different structural parameters to the amplitude of 2p space order 54 Hz radial electromagnetic force wave is analyzed. Based on the RBF neural network method, an approximate model between six different structural parameters and the amplitude of 2p space order 54 Hz radial electromagnetic force wave and average torque is established, and the motor is optimized by. The main conclusions are:

1) LHD test and parameters sensitivity analysis show that the air gap length and permanent magnet thickness have significant effects on the average torque and main radial electromagnetic force wave. The pole arc coefficient has a significant effect on the main radial electromagnetic force wave, but a small effect on the average torque. The tooth width has a greater effect on the average torque, but a smaller effect on the main radial electromagnetic force wave. The notch width and the slot depth have little effect on the average torque and the main radial electromagnetic force wave.
2) The results of motor optimization by NCGA show that reasonable selection of motor structural parameters such as pole arc coefficient, air gap length and permanent magnet thickness can not only effectively reduce the amplitude of the main radial electromagnetic force wave, but also improve the output capacity of the motor.

REFERENCES

[1] X. Bao, J. Liu, Y. Sun, and C. Wu, "Review and prospect of low-speed high-torque permanent magnet machines," *Trans. China Electrotech. Soc.*, vol. 34, no. 6, pp. 1148–1160, Mar. 2019.
[2] A. M. El-Refaie, "Fractional-slot concentrated-windings synchronous permanent magnet machines: Opportunities and challenges," *IEEE Trans. Ind. Electron.*, vol. 57, no. 1, pp. 107–121, Jan. 2010.
[3] W. Ma, D. Wang, S. Cheng, and J. Chen, "Common basic scientific problems and development of leading-edge technology of high performance motor system," *Proc. CSEE*, vol. 36, no. 8, pp. 3–13, Apr. 2016.
[4] T. Dong, W. Huang, and C. Wang, "Influence of unequal teeth tips width and alternate winding on torque characteristics in direct drive table motor," *Trans. China Electrotech. Soc.*, vol. 25, no. 8, pp. 12–17, Aug. 2010.
[5] H. Wang, Y. Yu, and D. Xu, "The position servo system of PMSM," *Proc. CSEE*, vol. 24, no. 7, pp. 155–159, Jul. 2004.
[6] C. Gerada, K. Bradley, C. Whitley, and G. Towers, "High torque density PM machines for high performance operation," in *Proc. 33rd Annu. Conf. IEEE Ind. Electron. Soc.*, Taiwan, 2007, pp. 210–215.
[7] A. M. El-Refaie, T. M. Jahns, and D. W. Novotny, "Analysis of surface permanent magnet machines with fractional-slot concentrated windings," *IEEE Trans. Energy Convers.*, vol. 21, no. 1, pp. 34–43, Mar. 2006.

[8] I. Petrov, M. Niemelä, P. Ponomarev, and J. Pyrhönen, "Rotor surface ferrite permanent magnets in electrical machines: Advantages and limitations," *IEEE Trans. Ind. Electron.*, vol. 64, no. 7, pp. 5314–5322, Jul. 2017.
[9] M. Valavi, A. Nysveen, R. Nilssen, R. D. Lorenz, and T. Rølvåg, "Influence of pole and slot combinations on magnetic forces and vibration in low-speed PM wind generators," *IEEE Trans. Magn.*, vol. 50, no. 5, pp. 1–11, May 2014.
[10] Y. Li, S. Li, J. Zhou, and L. Li, "Weakening approach of the vibration and noise based on the stator tooth chamfering in PMSM with similar number of poles and slots," *Trans. China Electrotech. Soc.*, vol. 30, no. 6, pp. 45–52, Mar. 2015.
[11] F. Lin, S. Zuo, Y. Mao, S. Wu, and W. Deng, "Semi-analytical model of vibration and noise for permanent magnet synchronous motor considering current harmonics," *Trans. China Electrotech. Soc.*, vol. 32, no. 9, pp. 24–31, May 2017.
[12] W. Su, D. Wang, K. Wei, N. Lin, X. Zhang, and Y. Guo, "Analysis of radial electromagnetic force wave of consequent-pole hybrid excitation synchronous generator," *Proc. CSEE*, vol. 40, no. 24, pp. 7869–7879, Dec. 2020.
[13] C. Lv, M. Li, and H. Chen, "Cogging frequency vibration of permanent magnet motor caused by zeroth-order radial magnetic forces," *Proc. CSEE*, vol. 41, no. 19, pp. 6778–6787, Oct. 2021.
[14] Z. Xing, X. Wang, W. Zhao, and G. Ma, "Calculation of electromagnetic force waves and analysis of stator vibration characteristics of surface Mount permanent magnet synchronous motor," *Proc. CSEE*, vol. 41, no. 14, pp. 5004–5013, Jul. 2021.
[15] S. Zuo, F. Lin, and X. Wu, "Noise analysis, calculation, and reduction of external rotor permanent-magnet synchronous motor," *IEEE Trans. Ind. Electron.*, vol. 62, no. 10, pp. 6204–6212, Oct. 2015.
[16] Z. Q. Zhu, Z. P. Xia, L. J. Wu, and G. W. Jewell, "Analytical modeling and finite-element computation of radial vibration force in fractional-slot permanent-magnet brushless machines," *IEEE Trans. Ind. Appl.*, vol. 46, no. 5, pp. 1908–1918, Sep. 2010.
[17] R. Zhang, X. Wang, D. Qiao, and Y. Yang, "Reduction of exciting force wave for permanent magnet motors by teeth notching," *Proc. CSEE*, vol. 30, no. 18, pp. 103–108, Jun. 2010.
[18] A. Cassat, C. Espanet, R. Coleman, L. Burdet, E. Leleu, D. Torregrossa, J. M'Boua, and A. Miraoui, "A practical solution to mitigate vibrations in industrial PM motors having concentric windings," *IEEE Trans. Ind. Appl.*, vol. 48, no. 5, pp. 1526–1538, Sep. 2012.
[19] F. Liu, X. Wang, Z. Xing, A. Yu, and C. Li, "Reduction of cogging torque and electromagnetic vibration based on different combination of pole arc coefficient for interior permanent magnet synchronous machine," *CES Trans. Electr. Mach. Syst.*, vol. 5, no. 4, pp. 291–300, Dec. 2021.
[20] K.-C. Kim, D.-H. Koo, J.-P. Hong, and J. Lee, "A study on the characteristics due to pole-arc to pole-pitch ratio and saliency to improve torque performance of IPMSM," *IEEE Trans. Magn.*, vol. 43, no. 6, pp. 2516–2518, Jun. 2007.
[21] A. Frias, P. Pellerey, A. K. Lebouc, C. Chillet, V. Lanfranchi, G. Friedrich, L. Albert, and L. Humbert, "Rotor and stator shape optimization of a synchronous machine to reduce iron losses and acoustic noise," in *Proc. IEEE Vehicle Power Propuls. Conf.*, Seoul, Korea (South), Oct. 2012, pp. 98–103.
[22] H. Kim and B. Kwon, "Optimal design of motor shape and magnetisation direction to obtain vibration reduction and average torque improvement in IPM BLDC motor," *IET Electric Power Appl.*, vol. 11, no. 3, pp. 378–385, Mar. 2017.
[23] S. Wang, J. Hong, Y. Sun, and H. Cao, "Analysis and reduction of electromagnetic vibration of PM brush DC motors," *IEEE Trans. Ind. Appl.*, vol. 55, no. 5, pp. 4605–4612, Sep. 2019.
[24] J. Wu, J. Wang, C. Gan, Q. Sun, and W. Kong, "Efficiency optimization of PMSM drives using field-circuit coupled FEM for EV/HEV applications," *IEEE Access*, vol. 6, pp. 15192–15201, 2018.
[25] M. Muteba, "Line-start synchronous reluctance motor with V-shaped rotor laminations," *IEEE Access*, vol. 10, pp. 109277–109288, 2022.

JIAKUAN XIA received the B.S., M.S., and Ph.D. degrees in electrical engineering from the Shenyang University of Technology, China, in 1986, 1997, and 2006, respectively. He is currently a Professor with the School of Electrical Engineering, Shenyang University of Technology. His research interests include modern motion control, power electronics, power transmission, design and research of large synchronous motor excitation systems, and design and control of special motor.

MEIJUN QI received the B.S. degree in electrical automatization from the Shenyang University of Technology, Shenyang, China, in 2020, where she is currently pursuing the joint M.S. and Ph.D. degrees with the School of Electrical Engineering. Her research interests include analysis and suppression of the vibration and noise of the motors.

TING DONG received the Ph.D. degree in electrical engineering from the Shenyang University of Technology, Shenyang, China, in 2010. Since 2011, she has been with the Electric Drive Research Institute, Shenyang University of Technology, where she is currently a Professor. Her major teaching activities and research interests include design and control of permanent magnet machines, especially those working in the high power density occasions.

MENGLIN SONG received the B.S. and M.S. degrees in electrical engineering from the Shenyang University of Technology, Shenyang, China, in 2012 and 2015, respectively. He is currently an Experimenter with the School of Electrical Engineering, Shenyang University of Technology. His research interests include power electronics, power transmission, and control of multiphase motor.